Available online at www.sciencedirect.com

SciVerse ScienceDirect

Ceramics International 39 (2013) 5561–5569

CERAMICS INTERNATIONAL

www.elsevier.com/locate/ceramint

Optimization of $Sm_{0.5}Sr_{0.5}CoO_{3-\delta}$–$Sm_{0.2}Ce_{0.8}O_{2-\delta}$ composite cathodes fabricated by electrostatic slurry spray deposition

Inyu Park[a], Jinyi Choi[a], Hunhyeong Lee[b], Dongwook Shin[a,b,*]

[a]Department of Fuel Cells and Hydrogen Technology, Hanyang University, 222 Wangsimni-ro, Seongdong-gu, Seoul 133-791, Republic of Korea
[b]Division of Materials Science & Engineering, Hanyang University, 222 Wangsimni-ro, Seongdong-gu, Seoul 133-791, Republic of Korea

Received 22 October 2012; received in revised form 13 December 2012; accepted 19 December 2012
Available online 28 December 2012

Abstract

Strontium doped samarium cobaltite ($Sm_{0.5}Sr_{0.5}CoO_{3-\delta}$, SSC)–samarium doped ceria ($Sm_{0.2}Ce_{0.8}O_{2-\delta}$, SDC) composite cathodes were fabricated using the electrostatic slurry spray deposition method for intermediate temperature solid oxide fuel cells (IT-SOFCs). To optimize the performance of the full cell containing the fabricated composite cathode, the effects of sintering temperature, composite ratio between SSC and SDC components, and film thickness of the composite cathode have been investigated through SEM, EDS and EIS analysis. As per the results, the best electrochemical performance was obtained from the SSC–SDC composite cathode sintered at 1000 °C in the weight ratio of 60:40 and with 20 μm in thickness. The cathode sintered at 1000 °C showed better performance than the cell sintered at 900 °C due to the well-developed connectivity between the SSC and the SDC particles. Also, the 60SSC–40SDC composite cathode showed an excellent percolating property and the lowest polarization resistance was obtained from the composite cathode with 20 μm in thickness due to its well developed microstructure in terms of gas diffusion and TPB area.

Keywords: SSC–SDC; Composite cathode; SOFC; Electrostatic slurry spray deposition

1. Introduction

Despite of its high efficiency and environmental friendliness, solid oxide fuel cell needs several critical improvements to commercialize [1]. The most important technical issue is the reduction of the operating temperature below 800 °C, where the electrochemical performance of the conventional YSZ based SOFC is also dramatically reduced [2,3]. To achieve the improved performance of SOFCs at low temperature, thin electrolyte and composite cathodes consisting of the cathode and the electrolyte materials have been suggested. Thin electrolyte can reduce ohmic resistance originating from the electrolyte [4–6], while the composite cathode can improve the electrode performance by expanding the active reaction sites, triple phase boundary (TPB), to whole cathode layer and reducing thermal expansion mismatch with the electrolyte [6–9]. The role of cathode becomes more important in the performance of SOFCs at the low or intermediate temperature range. Thus, the technique to prepare composite cathode is being studied to maximize the performance of the SOFCs.

$La_{1-x}Sr_xMnO_3$ (LSM) perovskite structure materials have been regarded as one of the promising cathode materials due to its fair ionic conductivity, as well as thermal and chemical stability [10,11]. While LSM has shown desirable performance for the SOFCs operating at temperature above 800 °C, its performance markedly deteriorates as the operating temperature is lowered. This is because the oxygen surface exchange coefficient and oxygen diffusion coefficient of LSM are relatively low [12,13]. To solve these problems, cobalt-containing perovskite materials have been explored in recent researches [12,14,15]. The cobalt-containing materials such as $Sm_{0.5}Sr_{0.5}CoO_3$ (SSC) [16], (La, Sr)CoO_3 (LSC) [17], (La, Sr)(Co, Fe)O_3 (LSCF) [18], and (Ba, Sr)(Co, Fe)O_3 (BSCF) [19] are mixed ionic and electronic conductors

*Corresponding author at: Division of Materials Science & Engineering, Hanyang University, 222 wangsimni-ro, Seongdong-gu, Seoul 133-791, Republic of Korea. Tel.: +82 2 2220 0503; fax: +82 2 2220 4011.
E-mail address: dwshin@hanyang.ac.kr (D. Shin).

0272-8842/$ - see front matter © 2012 Elsevier Ltd and Techna Group S.r.l. All rights reserved.
http://dx.doi.org/10.1016/j.ceramint.2012.12.070

(MIECs) and they tend to exhibit higher ionic conductivities than LSM due to greater concentration of oxygen vacancies, which enable the extension of electrochemically active area from just the triple phase boundary (TPB) to the entire MIECs layer [20]. Among the above mentioned materials, SSC is regarded as one of the promising cathode materials because it exhibits extraordinary electronic conductivity than that of pure BSCF [19] and good catalytic activity for oxygen reduction [21]. Ishihara et al. [22] and Fukunaga et al. [23] reported that the overpotential of dense SSC film is lower than that of the LSC film under the same condition due to the fact that the oxygen adsorption–desorption rate of SSC is one order magnitude higher than dense LSC. Furthermore, the electrochemical performance of SSC porous cathode can be improved by adding samarium doped ceria ($Sm_{0.2}Ce_{0.8}O_{1.9}$, SDC), since addition of SDC to SSC cathode is beneficial by narrowing the difference of thermal expansion coefficients between the electrolyte and cathode. SSC is also known to be compatible both chemically and physically with ceria based electrolytes [16].

In this research, strontium doped samarium cobaltite ($Sm_{0.5}Sr_{0.5}CoO_{3-\delta}$, SSC) and samarium doped ceria ($Sm_{0.2}Ce_{0.8}O_{1.9}$, SDC) composite cathodes were fabricated by using the electrostatic slurry spray deposition (ESSD). The ESSD technique uses electrical energy to atomize and spray solutions same as in electrostatic spray deposition (ESD). However, the ESSD technique is a method of spraying prepared slurry containing powders with pre-developed crystalline phase, while the conventional ESD is a technique of spraying metal salts dissolved solution and the crystalline phases are developed after deposition by post-heat treatment. Dense and porous films without any cracks and delamination can be easily fabricated by the ESSD [24,25]. Also, it is very powerful tool to fabricate a layer with composite materials and to control film thickness. In overall, the ESSD is a more advanced deposition technique than the conventional ESD in terms of the controllability of the deposition process and the microstructure of the deposited film, the flexibility in process application, the performance of the obtained film, the diversity of film material, so on.

To optimize the cell performance containing SSC–SDC composite cathode, various experimental variables and the resulting microstructural and electrochemical characteristics of the composite cathode were investigated. The variables were the microstructural features such as the triple phase boundary and the connectivity between the particles, composite ratio of the SSC and SDC and its film thickness. The influence of the composite cathode on the electrochemical properties was studied using electrochemical impedance spectroscopy.

2. Experimental procedure

2.1. Slurry preparation

To prepare a SSC–SDC composite slurry, strontium doped samarium cobaltite (SSC, Winner Tech., Republic of Korea) and samarium doped ceria (SDC, Fuel cell materials, USA) were used as solid constituents. The average particle sizes were about 300 nm for the SSC and 30 nm for the SDC. Isopropyl alcohol (IPA) and toluene (Daejung Chemicals & Metals Co. Ltd., Republic of Korea) as solvents and polyvinyl butyral (PVB, Sigma-Aldrich, USA) as a dispersant were used. Firstly, IPA and toluene were mixed with volume ratio of 7:3 and then, 3 wt% PVB of the amount of solid loading was diluted in the pre-mixed solvent. The prepared SSC and SDC powders were, subsequently, added into the PVB diluted solvent. The weight ratio of the SSC and SDC powders was varied to investigate the influence of the composite ratio of the SSC–SDC cathode on the electrochemical properties. Furthermore, ultra-sonication was carried out for 1 h to enhance the dispersion stabilization of the SSC–SDC composite slurry.

2.2. Fabrication of composite cathodes

To investigate the various effects of the composite cathode, various specimens with different microstructures were fabricated using the electrostatic slurry spray deposition (ESSD). The ESSD system is constructed with a syringe pump to feed the prepared composite slurry, a power supply with high voltage to atomize and spray the fed slurry, and stainless nozzle to form the electric field. The detailed schematic diagram of the ESSD system is shown in Fig. 1. The applied voltage and flow were 11 kV and 6 mL/h, respectively. The distance between nozzle and substrate was 5 cm. Whole deposition process for the composite cathode was conducted in an ambient atmosphere and no substrate heating. The slurries for composite cathodes were sprayed and deposited onto the SDC pellets, which were uni-axially pelletized to the disc with 13 mm in diameter and 1 mm in thickness, then subsequently sintered at 1400 °C for 2 h in an electric furnace. After sintering the pellets were shrunk to ~10 mm in diameter. In addition, the spray was carried out under the cone-jet mode [26] and the spray covered area of ~80 mm in diameter. After deposition, the SSC–SDC composite cathodes were

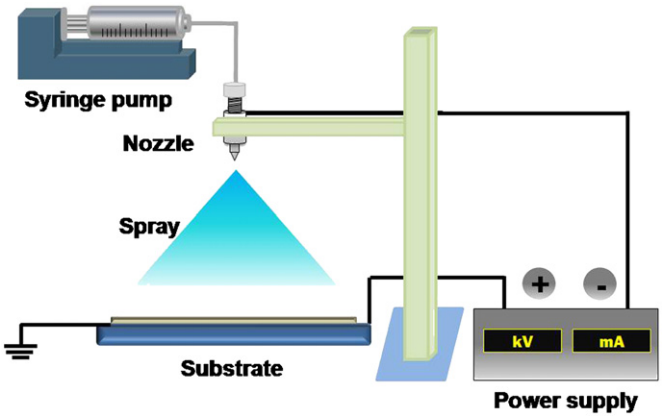

Fig. 1. Schematic diagram of the electrostatic slurry spray deposition (ESSD) system.

sintered at 900 °C and 1000 °C for 5 min in a microwave furnace (2.45 GH, 2 kW) to study the influence of the sintering temperature on the microstructure and electrochemical performance of the composite cathodes. In order to measure and control the sintering temperature, the thermocouple was placed at diagonal direction from the specimen and the distance was ~3 cm.

2.3. Characterization

With the prepared SSC–SDC composite cathodes, the microstructural change and crystallinity of the specimens as a function of sintering temperature, film thickness and composite ratio of the SSC and SDC were observed with scanning electron microscopy (SEM, JEOL JCM-5700, Japan) and X-ray diffractometer (XRD, Rigaku Rint 2000, Japan). Also, AC impedance spectroscopy was applied to examine the electrochemical performance with Solatron SI 1260 frequency response analyzer and 1287 electrochemical interface. The impedance spectra were recorded with three electrode configuration cell under open circuit condition using a 20 mV amplitude AC signal over a frequency range from 1 MHz to 0.01 Hz. Platinum paste was painted as a counter and a reference electrode and sintered at 850 °C for 5 min in the microwave furnace. Also, it was measured in the temperature range between 600 and 750 °C with an increment of 50 °C in air.

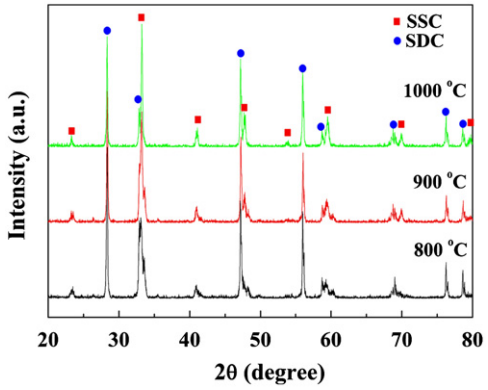

Fig. 2. X-ray diffraction patterns of the 80SSC–20SDC composite cathodes at various sintering temperatures.

3. Results and discussion

3.1. The effect of sintering temperature

Fig. 2 shows the crystallinity of 80 wt% of SSC–20 wt% of SDC (80SSC–20SDC) composite cathodes at various sintering temperatures. The pure perovskite structure of SSC and fluorite structure of SDC were developed over 900 °C, while some SSC peaks appeared weakly below 900 °C. As a result, sintering temperatures of 900 °C and 1000 °C were selected to compare the electrochemical property originated from different microstructures such as TPB and connectivity. The microstructures of the SSC–SDC composite cathodes fabricated by the ESSD technique are shown in Fig. 3. The morphologies of the composite cathode sintered at 900 °C seem to have large TPB area, but low connectivity between each particle as shown in Fig. 3(a) and (c). On the other hand, Fig. 3(b) and (d) shows the microstructures of the sample sintered at 1000 °C. It is observed that the sample has well developed connectivity between each particle, but the grain size is bigger compared to the cathode sintered at 900 °C. Moreover, the composite cathode adhered well to the electrolyte surface as shown in the inset of Fig. 3(d). Fig. 4 shows the

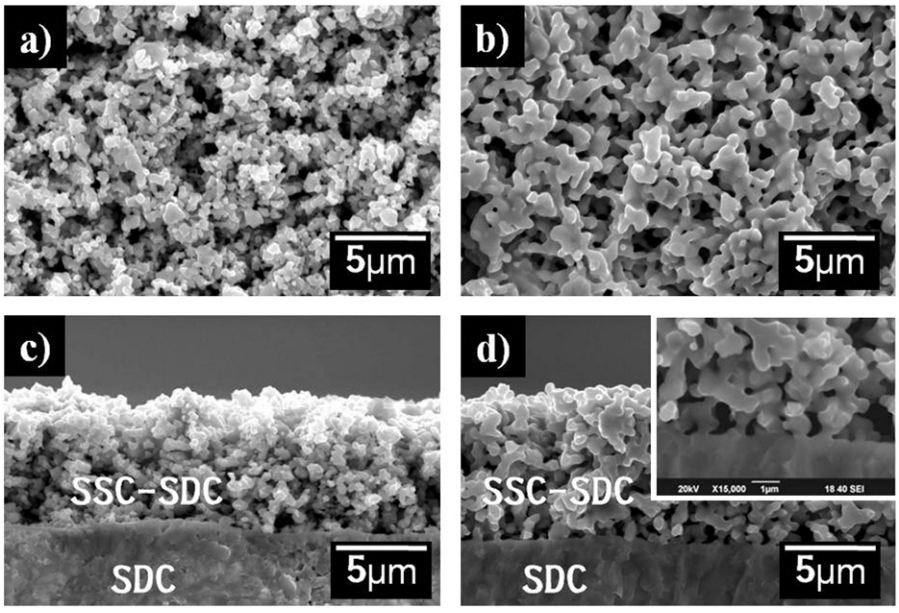

Fig. 3. Microstructural images of the SSC–DC (8:2 in weight percent) composite cathodes, (a) surface and (c) cross-sectional images sintered at 900 °C and (b) surface and (d) cross-sectional images sintered at 1000 °C.

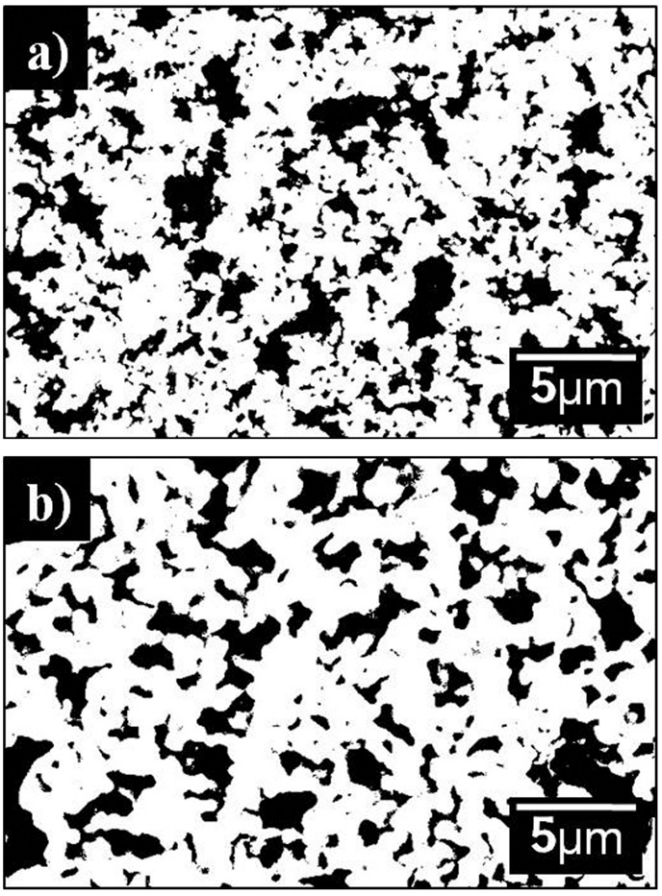

Fig. 4. Different connectivity and TPB area of the samples analyzed by image analysis program; sintered at (a) 900 °C and (b) 1000 °C.

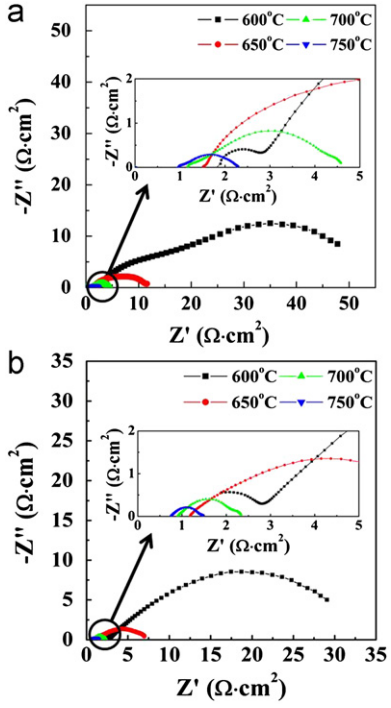

Fig. 5. AC impedance spectra of the samples sintered at (a) 900 °C and (b) 1000 °C.

connectivity and porosity of each sample with surface microstructures analyzed by image analysis program (Image Pro Plus). Two specimens show very clear

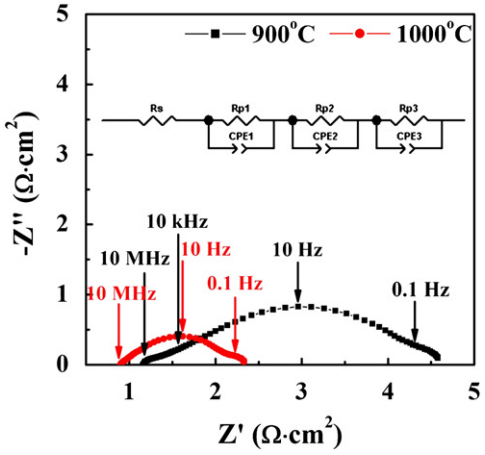

Fig. 6. Comparison of the polarization resistances and equivalent circuit (inset) of the electrode reaction measured at 700 °C.

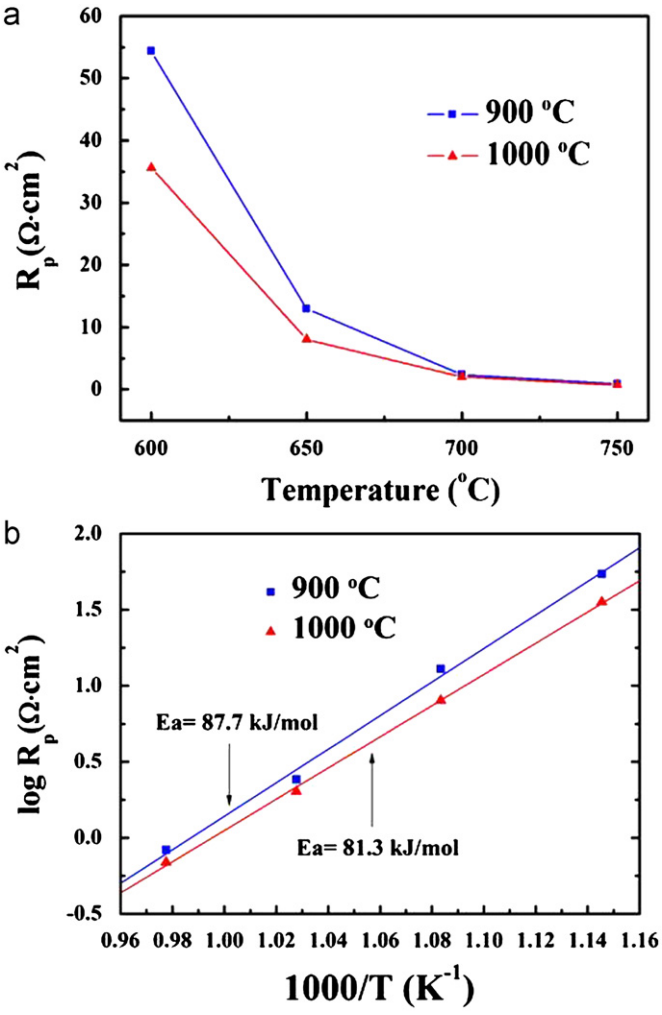

Fig. 7. (a) Polarization resistances and (b) conductivities of the 80SSC–20SDC composite cathodes sintered at 900 and 1000 °C.

differences in the connectivity and the TPB area. These differences resulted from the sintering temperature and the grain growth of the composite particles. For these two samples, the AC impedance measurement was carried out to compare the electrochemical property. Fig. 5 shows typical impedance spectra for the two samples measured in air at 650–750 °C. It is noteworthy that the polarization resistance of the specimen sintered at 1000 °C is lower than the one sintered at 900 °C in whole temperature range. The polarization resistances measured at 700 °C were compared as shown in Fig. 6 and the obtained impedance spectra could be fitted to three distinct semi circles represented by an equivalent circuit shown in inset figure in Fig. 6. The equivalent circuit consisted of $R_s(R_{p1}\,CPE_1)(R_{p2}\,CPE_2)(R_{p3}\,CPE_3)$, when R_s is the ohmic resistance of the electrolyte, CPE_1, CPE_2, CPE_3 are constant phase elements, and R_{p1}, R_{p2}, R_{p3} are the polarization resistances of cathodes for high, middle, and low frequency range, respectively. From the result, it can be seen that R_{p1} (high frequency) and R_{p2} (middle frequency) were remarkably decreased at the sample sintered at 1000 °C than that sintered at 900 °C. It is well know that the polarization resistances at high and middle frequency corresponded to the charge transfer of oxygen ions at interface between electrolyte and electrode and surface diffusion of adsorbed oxygen species, respectively [27]. Fig. 7 indicates the polarization resistances and temperature dependences of the polarization resistance for the SSC–SDC composite cathodes. The activation energy was also lower than the composite cathode sintered at 900 °C. This result means that connectivity is the critical factor to enhance performance of the SOFCs. Thus, for the nano-porous structure, TPB and the necking structure between each particle have to be properly optimized simultaneously. In this study, the optimum sintering temperature was verified at 1000 °C for the SSC–SDC composite cathode.

3.2. The effect of composite ratio

To optimize the SSC–SDC composite ratio, three cathode films with different composite ratios were sintered at 1000 °C and the electrochemical performances were measured. Fig. 8 depicts the microstructures of the fabricated SSC–SDC composite cathodes, which were composed of various SSC–SDC composite ratios. Their chemical compositions analyzed by energy dispersive spectrometer (EDS) are listed in Table 1. Weight percentage of all elements in the fabricated cathode films were close to the intended stoichiometric values, which suggests that the ESSD technique is very stable to transfer the stoichiometric ratio of slurry to film. As shown in Fig. 8, the microstructures have been slightly changed from the structure (Fig. 8(a)) with small grain size and expanded TPB area to the one (Fig. 8(e)) with relatively large grain

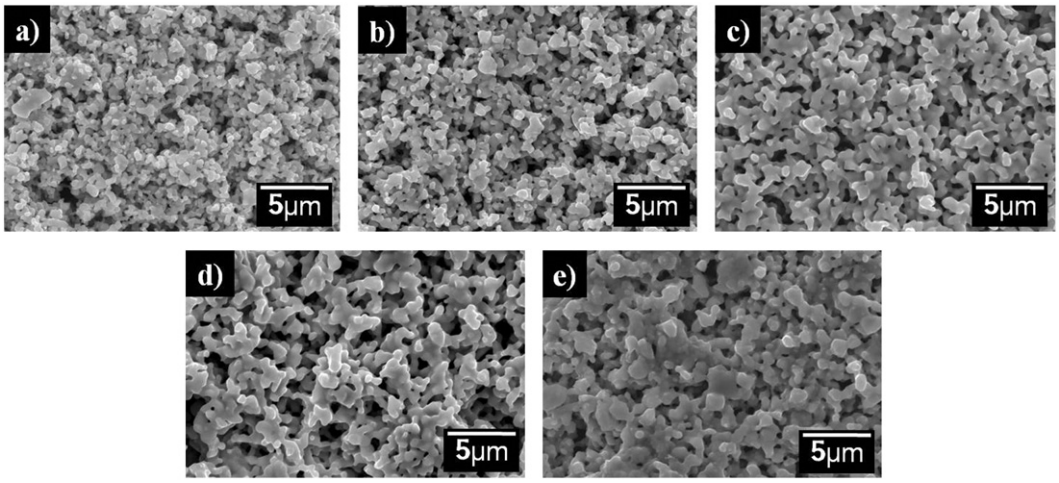

Fig. 8. SEM images of the SSC–SDC composite cathodes with different composite ratios; (a) 100SSC, (b) 80SSC–20SDC, (c) 70SSC–30SDC, (d) 60SSC–40SDC and (e) 50SSC–50SDC.

Table 1
Chemical compositions of the three different SSC–SDC composite cathodes.

	Composition of powder (wt%)				
	100SSC	80SSC–20SDC	70SSC–30SDC	60SSC–40SDC	50SSC–50SDC
Sm	42.3	38	36.3	34.1	31.7
Sr	24.6	19.7	17.2	14.7	12.3
Co	33.1	26.5	23.1	19.7	16.6
Ce	–	15.8	23.4	31.5	39.4

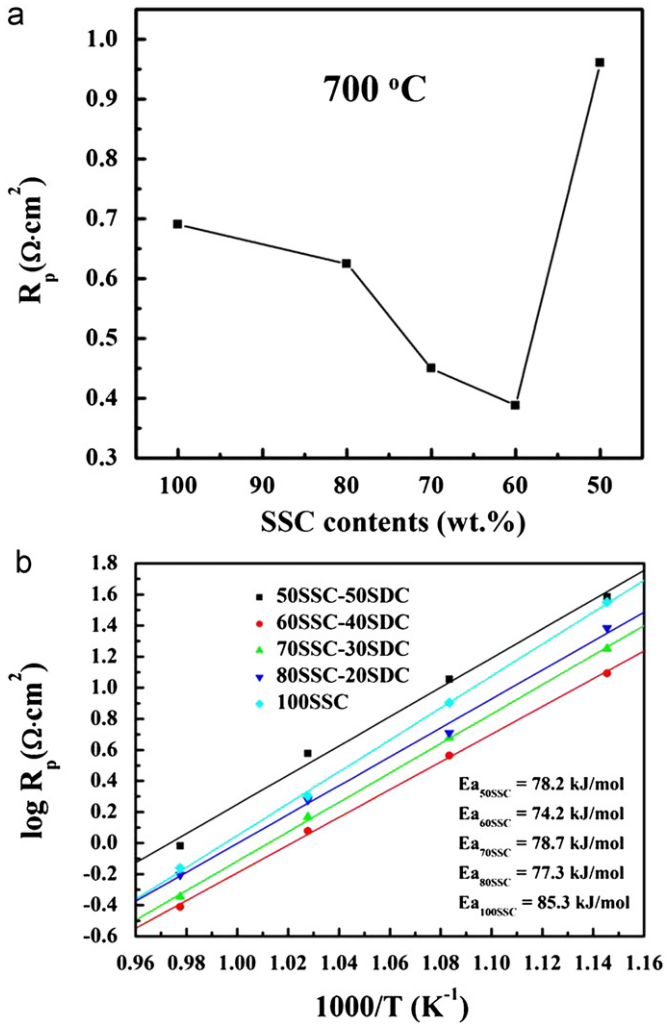

Fig. 9. (a) Polarization resistances of the SSC–SDC composite cathodes measured at 700 °C and (b) their electrical conductivities with different composite ratios.

and well connected to each particle as increasing SDC contents in the cathode. It is well known that nano-sized particles exhibit faster grain growth than micro-sized particles even at lower temperature [28]. The mean particle size of the SDC powder used in this study was about 30 nm. Thus, it is considered that this microstructural evolution was yielded due to nano-size effect of the SDC particles. Fig. 9 represents the polarization resistances and electrical conductivities for the SSC–SDC composite cathodes with different composite ratios. As shown in Fig. 9(a), the polarization resistance measured at 700 °C decreased with increasing SDC contents up to 60 wt%. However, the polarization resistance of the 50SSC–50SDC composite cathode drastically increased even higher than 100SSC cathode. Also, the activation energy was gradually decreased from 85.3 kJ/mol for the 100SSC cathode to 74.2 kJ/mol for the 60SSC–40SDC composite cathode. This phenomenon can be explained with the percolation theory [29–31]. The percolation represents the possibility that particles are clustered forming connected conduction pathways. The concept of coordination numbers is important to practical understanding of the percolation theory. In general, the coordination number represents the number of contacts or neighboring particles. Conceptual graphical explanation is depicted in Fig. 10. The SDC electrolyte particles were mixed to the electrode to enhance ionic conduction. Continuous increase of the SDC particles gradually forms the conduction pathways for the ionic conduction and, finally, helps the ionic conduction of adsorbed and dissociated oxygen ions in the cathode. Therefore it is reasonable to assume that the ionic and electronic conduction pathways penetrating from the cathode surface to the electrolyte are fully constructed in the sample of 60SSC–40SDC composite cathode. However, excessive SDC particles in the composite cathode could act as insulating barrier to the electronic conduction by isolating SSC particles. The drastic increase of the polarization resistance in the 50SSC–50SDC composite cathode could be explained by the above mentioned reason. The optimum composite ratio of the SSC–SDC cathode was studied to 60SSC–40SDC.

3.3. The effect of film thickness

For the enhancement of fuel cell performance, careful thicknesses control of the composite cathode films is required because rate determining step could be changed by evolution of dominant polarization resistance of a cathode film. Fig. 11 shows the microstructures of the SSC–SDC composite cathodes with different thickness. All composite cathode films were fabricated using the ESSD technique with variable deposition time. All depositions were carried out at a cone-jet mode with 5 mL/h of slurry feeding rate, 6.5 cm of nozzle to substrate distance and no substrate heating. To investigate the effect of film thickness, five different composite cathodes with 2.5 μm to ~30 μm in thickness were prepared. The compositional ratio of the SSC and SDC was 60:40 in weight percent and all specimens were sintered at 1000 °C. As shown in Fig. 11, the microstructures are porous and uniform and the connectivity is well developed between each neighboring particle. Fig. 12 shows the film thickness change of the SSC–SDC composite cathodes deposited by the ESSD technique. The deposition rate is almost 1 μm/min and shows linear relationship to deposition time. The electrochemical properties of the composite cathodes are shown in Fig. 13. The polarization resistances at each measuring temperature decreased with increasing film thickness from ~2.5 μm to ~20 μm, then, sharply increased again in the composite cathode with ~30 μm in thickness. Also, the lowest activation energy was obtained from the specimen with ~20 μm cathode film and it was 62.9 kJ/mol. On the other hand, the cathode with ~2.5 μm thickness showed the worst performance. The cathode performance deteriorates significantly when a large particle size is used in conjunction with a thin electrode. This poor performance in the SSC–SDC composite cathode with ~2.5 μm in thickness is mainly caused due

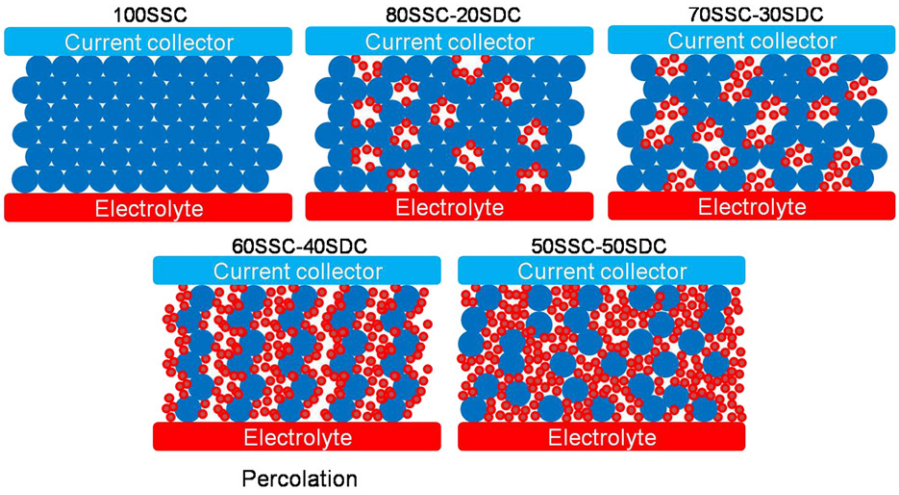

Fig. 10. Schematic diagram of SSC–SDC composite cathodes with various SDC content. The blue particles represent the SSC electrode particles and the red particles represent the SDC electrolyte. (For interpretation of the references to color in this figure legend, the reader is referred to the web version of this article.)

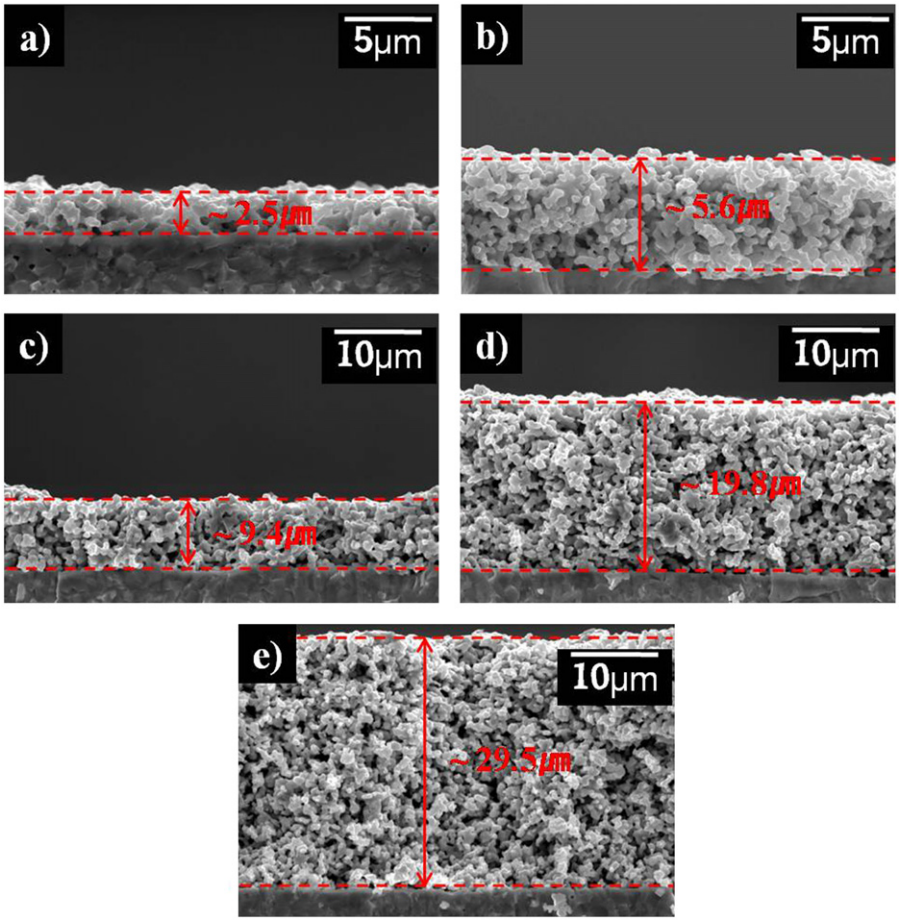

Fig. 11. The cross sectional images of the 60SSC–40SDC composite cathode films with various thicknesses.

to insufficient reaction sites for the electrochemical performance compared to other cathodes. Thus, the performance of thicker cathode could be improved with increase of the sufficient reaction sites until the thickness reaches to an optimum point. If the thickness, however, becomes thicker than the optimum point, the polarization could be increased again due to the too long charge pathways and the difficulty in gas diffusion into the cathode interior nearby the interface between electrode and electrolyte. In other words, the electrical conductivity could be attenuated when the cathode thickness becomes very thin due to insufficient TPB area between three components (electrode, electrolyte and gas).

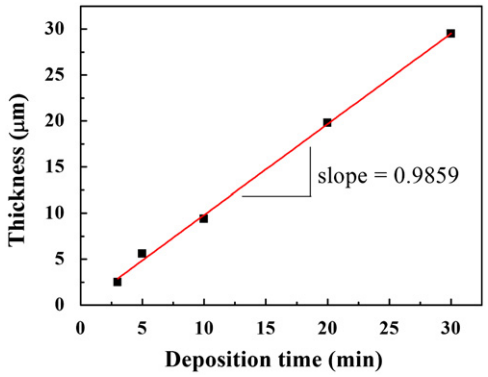

Fig. 12. The film thickness of the SSC–SDC composite cathode as a function of deposition time.

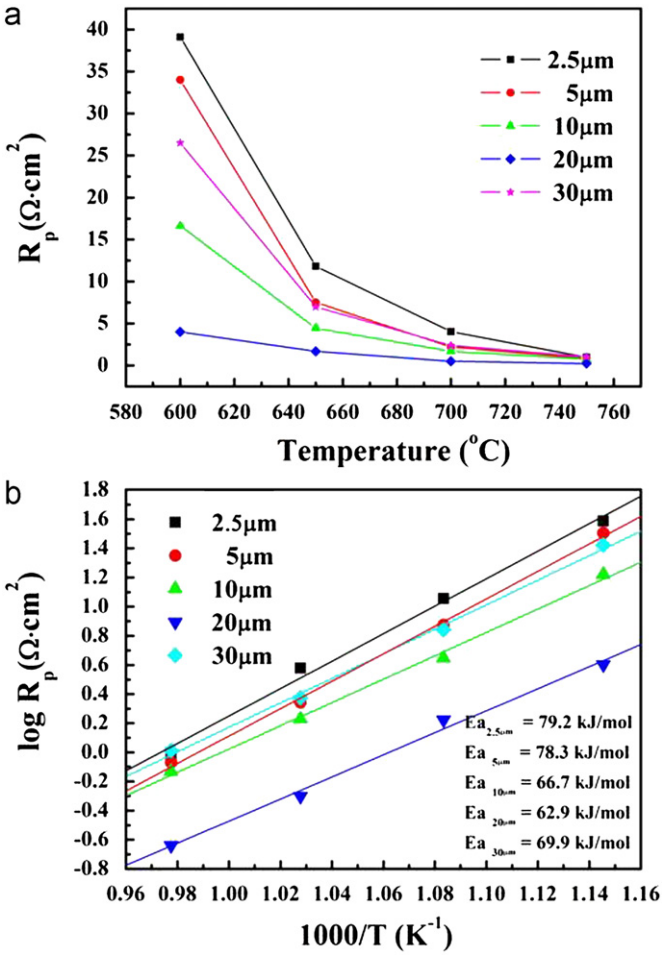

Fig. 13. (a) polarization resistances and (b) Arrhenius plots of the 60SSC–40SDC composite cathodes with various thicknesses.

Also, it could be decreased when the cathode film is too thick due to the fact that polarization resistances caused by surface diffusion of oxygen ions in the cathode bulk or gas diffusion from the cathode surface to the interface are increased. This result agrees well to the previous research. Chan et al. [32] reported that the cathodic overpotential and cell performance were significantly influenced by the cathode thickness and the high overpotential occurs when the thickness becomes either very thin or very thick because of the small amount of the active reaction site or higher flow resistance in conjunction with higher ohmic losses. Therefore, the cathode thickness is required to be optimized considering the TPB and gas diffusion in the composite cathodes. In this study, it is confirmed that the optimized SSC–SDC composite cathode thickness is ~20 μm.

4. Conclusions

In this study, the SSC–SDC composite cathodes were successfully fabricated using the electrostatic slurry spray deposition (ESSD). It is demonstrated that the ESSD system is a promising technique for fabrication of porous and composite films. The prepared SSC–SDC composite cathodes were optimized considering the effects of sintering temperature, composite ratio between SSC and SDC powders, and thickness. The most promising performance was obtained from the SSC–SDC composite cathode with about 20 μm in thickness sintered at 1000 °C, which was composed of 60 wt% of the SSC and 40 wt% of the SDC. Its polarization resistance was 0.23 Ω cm^2 and the activation energy was 62.9 kJ/mol, respectively.

Acknowledgments

This research was supported by the Fusion Research Program for Green Technologies through the National Research Foundation of Korea (NRF) funded by the Ministry of Education, Science and Technology (2011-0019319). Also, this work is the outcome of a Manpower Development Program for Energy supported by the Ministry of Knowledge and Economy (MKE).

References

[1] A. Atkinson, S. Barnett, R.J. Gorte, J.T.S. Irvine, A.J. McEvoy, M. Mogensen, S.C. Singhal, J. Vohs, Advanced anodes for high-temperature fuel cells, Nature Materials 3 (2004) 17–27.
[2] Y.J. Leng, S.H. Chan, K.A. Khor, S.P. Jiang, Performance evaluation of anode-supported solid oxide fuel cells with thin film YSZ electrolyte, International Journal of Hydrogen Energy 29 (2004) 1025–1033.
[3] X. Xu, C. Xia, S. Huang, D. Peng, YSZ thin films deposited by spin-coating for IT-SOFCs, Ceramics International 31 (2005) 1061–1064.
[4] S. De Souza, S.J. Visco, L.C. De Jonghe, Thin-film solid oxide fuel cell with high performance at low-temperature, Solid State Ionics 98 (1997) 57–61.
[5] C. Xia, F. Chen, M. Liu, Reduced-temperature solid oxide fuel cells fabricated by screen printing, Electrochemical and Solid-State Letters 4 (2001) A52–A54.
[6] S.M. Haile, Fuel cell materials and components, Acta Materialia 51 (2003) 5981–6000.
[7] V. Dusastre, J.A. Kilner, Optimisation of composite cathodes for intermediate temperature SOFC applications, Solid State Ionics 126 (1999) 163–174.
[8] E. Perry Murray, M.J. Sever, S.A. Barnett, Electrochemical performance of (La,Sr)(Co,Fe)O_3–(Ce,Gd)O_3 composite cathodes, Solid State Ionics 148 (2002) 27–34.

[9] J. Deseure, Y. Bultel, L. Dessemond, E. Siebert, Theoretical optimisation of a SOFC composite cathode, Electrochimica Acta 50 (2005) 2037–2046.
[10] S.C. Singhal, Advances in solid oxide fuel cell technology, Solid State Ionics 135 (2000) 305–313.
[11] X. Xu, C. Cao, C. Xia, D. Peng, Electrochemical performance of LSM–SDC electrodes prepared with ion-impregnated LSM, Ceramics International 35 (2009) 2213–2218.
[12] B.C.H. Steele, Appraisal of $Ce_{1-y}Gd_yO_{2-y/2}$ electrolytes for IT-SOFC operation at 500 °C, Solid State Ionics 129 (2000) 95–110.
[13] R. Doshi, L. Von Richards, J.D. Carter, X. Wang, M. Krumpelt, Development of solid-oxide fuel cells that operate at 500 °C, Journal of the Electrochemical Society 146 (1999) 1273–1278.
[14] E. Maguire, B. Gharbage, F.M.B. Marques, J.A. Labrincha, Cathode materials for intermediate temperature SOFCs, Solid State Ionics 127 (2000) 329–335.
[15] V. Dusastre, J.A. Kilner, Optimisation of composite cathodes for intermediate temperature SOFC applications, Solid State Ionics 126 (1999) 163–174.
[16] C. Xia, W. Rauch, F. Chen, M. Liu, $Sm_{0.5}Sr_{0.5}CoO_3$ cathodes for low-temperature SOFCs, Solid State Ionics 149 (2002) 11–19.
[17] S. Zha, W. Rauch, M. Liu, Ni–$Ce_{0.9}Gd_{0.1}O_{1.95}$ anode for GDC electrolyte-based low-temperature SOFCs, Solid State Ionics 166 (2004) 241–250.
[18] W.G. Wang, M. Mogensen, High-performance lanthanum-ferrite-based cathode for SOFC, Solid State Ionics 176 (2005) 457–462.
[19] W. Zhu, Z. Lü, S. Li, B. Wei, J. Miao, X. Huang, K. Chen, N. Ai, W. Su, Study on $Ba_{0.5}Sr_{0.5}Co_{0.8}Fe_{0.2}O_{3-\delta}$–$Sm_{0.5}Sr_{0.5}CoO_{3-\delta}$ composite cathode materials for IT-SOFCs, Journal of Alloys and Compounds 465 (2008) 274–279.
[20] X. Zhang, M. Robertson, S. Yick, C. Deĉes-Petit, E. Styles, W. Qu, Y. Xie, R. Hui, J. Roller, O. Kesler, R. Maric, D. Ghosh, $Sm_{0.5}Sr_{0.5}CoO_3+Sm_{0.2}Ce_{0.8}O_{1.9}$ composite cathode for cermet supported thin $Sm_{0.2}Ce_{0.8}O_{1.9}$ electrolyte SOFC operating below 600 °C, Journal of Power Sources 160 (2006) 1211–1216.
[21] F.S. Baumann, J. Maier, J. Fleig, The polarization resistance of mixed conducting SOFC cathodes: a comparative study using thin film model electrodes, Solid State Ionics 179 (2008) 1198–1204.
[22] T. Ishihara, M. Honda, T. Shibayama, H. Minami, H. Nishiguchi, Y. Takita, Intermediate temperature solid oxide fuel cells using a new $LaGaO_3$ based oxide ion conductor, Journal of the Electrochemical Society 145 (1998) 3177–3183.
[23] H. Fukunaga, M. Koyama, N. Takahashi, C. Wen, K. Yamada, Reaction model of dense $Sm_{0.5}Sr_{0.5}CoO_3$ as SOFC cathode, Solid State Ionics 132 (2000) 279–285.
[24] J. Choi, I. Park, H. Lee, D. Shin, Effect of enhanced reaction area in double layered $Ba_{0.5}Sr_{0.5}Co_{0.8}Fe_{0.2}O_{3-\delta}$ cathode for intermediate temperature solid oxide fuel cells, Solid State Ionics 216 (2012) 54–57.
[25] J. Lee, I. Park, H. Lee, D. Shin, Effects of embossing structure on the performance of intermediate-temperature solid oxide fuel cells with gadolinium-doped ceria electrolyte, Journal of Power Sources 212 (2012) 35–42.
[26] H.-H. Kim, J.-H. Kim, A. Ogata, Time-resolved high-speed camera observation of electrospray, Journal of Aerosol Science 42 (2011) 249–263.
[27] N. Grunbaum, L. Dessemond, J. Fouletier, F. Prado, A. Caneiro, Electrode reaction of $Sr_{1-x}La_xCo_{0.8}Fe_{0.2}O_{3-\delta}$ with $x=0.1$ and 0.6 on $Ce_{0.9}Gd_{0.1}O_{1.95}$ at $600 \le T \le 800$ °C, Solid State Ionics 177 (2006) 907–913.
[28] J.-S. Lee, J.-H. Mun, B.-D. Han, H.-D. Kim, B.-C. Shin, I.-S. Kim, Effect of raw-Si particle size on the properties of sintered reaction-bonded silicon nitride, Ceramics International 30 (2004) 965–976.
[29] S. Sunde, Monte Carlo simulations of polarization resistance of composite electrodes for solid oxide fuel cells, Journal of the Electrochemical Society 143 (1996) 1930–1939.
[30] P. Costamagna, M. Panizza, G. Cerisola, A. Barbucci, Effect of composition on the performance of cermet electrodes. Experimental and theoretical approach, Electrochimica Acta 47 (2002) 1079–1089.
[31] D.H. Jeon, J.H. Nam, C.J. Kim, Microstructural optimization of anode-supported solid oxide fuel cells by a comprehensive microscale model, Journal of the Electrochemical Society 153 (2006) A406–A417.
[32] S.H. Chan, X.J. Chen, K.A. Khor, Cathode micromodel of solid oxide fuel cell, Journal of the Electrochemical Society 151 (2004) A164–A172.